



Shortwave radiative forcing and feedback to the surface by sulphate geoengineering: Analysis of the Geoengineering Model Intercomparison Project G4 scenario

Hiroki Kashimura¹, Manabu Abe¹, Shingo Watanabe¹, Takashi Sekiya¹, Duoying Ji², John C. Moore², Jason N. S. Cole³, and Ben Kravitz⁴

¹Japan Agency for Marine-Earth Science and Technology, Yokohama, Japan.

²College of Global Change and Earth System Science, Beijing Normal University, Beijing, China.

³Canadian Centre for Climate Modelling and Analysis, Environment and Climate Change Canada, Victoria, British Columbia, Canada.

⁴Atmospheric Sciences and Global Change Division, Pacific Northwest National Laboratory, Washington, USA.

Correspondence to: Hiroki Kashimura (hiroki.kashimura@jamstec.go.jp)

Abstract. This study evaluates the forcing and feedback of net shortwave radiation at the surface in the G4 experiment of the Geoengineering Model Intercomparison Project by analysing outputs from six participating models. G4 involves injection of 5 Tg yr⁻¹ of SO₂, a sulphate aerosol precursor, into the lower stratosphere from year 2020 to 2070 against a background scenario of RCP4.5. A single layer atmospheric model for shortwave radiative transfer is used to estimate the direct forcing of solar radiation management (SRM) and feedback effects from changes in the water vapour amount, cloud amount, and surface albedo (compared with RCP4.5). The analysis shows that the globally and temporally averaged SRM forcing ranges from -3.6 to -1.6 W m⁻², depending on the model. The feedback effects due to changes in the water vapour and cloud amounts on net shortwave radiation have heating effects ranging from approximately 0.4 to 1.5 W m⁻² and weaken the effect of SRM by around 50 %. The surface albedo changes have a cooling effect, which is locally strong (~ 4 W m⁻²) in snow and sea ice melting regions, but minor for the global average. The analyses show that the results of the G4 experiment, which simulates sulphate geoengineering, include large inter-model variability both in the direct SRM forcing and the feedback from changes in the cloud amount, and imply a high uncertainty in modelled processes of sulphate aerosols and clouds.

1 Introduction

Geoengineering, or climate engineering, is the deliberate large-scale manipulation of the planetary environment to counteract anthropogenic climate change (e.g., Shepherd, 2009). One major category of geoengineering for lessening the effects of global warming is solar radiation management (SRM), which aims to reduce the amount of solar radiation at the Earth's surface. One of several SRM approaches (e.g., Lane et al., 2007) is to mimic a volcanic eruption by injecting sulphate aerosol precursors, such as SO₂, into the stratosphere (e.g., Budyko, 1974; Crutzen, 2006); this approach is called sulphate geoengineering. Large volcanic eruptions carry SO₂ gases into the stratosphere; these gases are photo-chemically oxidized to form sulphate aerosols, which have high reflectivity in the visible and ultraviolet regions of the electromagnetic spectrum. Sulphate aerosols increase



the solar reflectivity of the atmosphere, decreasing the shortwave radiation (SW) reaching the surface, and therefore cooling the air temperature. For example, the 1991 eruption of Mount Pinatubo reduced the globally averaged surface air temperature by up to 0.5 K (Parker et al., 1996).

To explore the cooling effect of and the climate responses from sulphate geoengineering, or more generally SRM, several climate-modelling groups performed various experiments using global climate models or Earth System Models (ESMs). Some experiments involved simplifying the net effects of SRM by reducing the solar constant. Govindasamy and Caldeira (2000) and Bala et al. (2008) performed a CO₂ doubling experiment with a 1.8 % reduction of the solar constant, and showed that such a decrease would compensate the global mean temperature change caused by the CO₂ doubling in their models. Govindasamy et al. (2002) considered the impact of the solar constant reduction on the terrestrial biosphere, whilst a CO₂ quadrupling experiment with a 3.6 % reduction of the solar constant was explored in Govindasamy et al. (2003). Furthermore, Matthews and Caldeira (2007) adopted the IPCC A2 scenario (IPCC, 2007) as their reference simulation and performed experiments in which the geoengineering was applied for different years. Others have simulated sulphate geoengineering with models that can calculate the production of sulphate aerosols from the injected SO₂ and the dynamical transportation. For example, Rasch et al. (2008) designed their experiments with SO₂ injection by 1–2 Tg S yr⁻¹ in an equatorial region with doubled CO₂, whereas Robock et al. (2008) adopted the A1B scenario as their baseline run and injected 3–10 Tg S yr⁻¹ of SO₂ from arctic or tropical regions in their simulation. Most of the aforementioned studies used different forcing and/or schemes for geoengineering, different scenarios for the baseline, and different models. Therefore, it is difficult to compare these studies or evaluate the uncertainty in the geoengineering simulations. However, Jones et al. (2010) compared the results of two different models in an experiment similar to that of Robock et al. (2008). They showed the different responses by the two models and emphasized the importance of intercomparing many different climate models with a common experimental design in order to assess the impact of the geoengineering.

The Geoengineering Model Intercomparison Project (GeoMIP) (Kravitz et al., 2011) was established to coordinate simulations with a common framework and to determine the robust effects and responses to geoengineering processes. For the first series of GeoMIP experiments, four experiments named G1, G2, G3, and G4 were proposed. The first two are designed to counteract quadrupled CO₂ radiative forcing (G1) and a 1 % increase in the CO₂ concentration per year (G2) by simply reducing the solar constant. The last two are designed to inject SO₂ into the lower stratosphere and decrease SW flux reaching the surface by increasing the SW reflection by sulphate aerosols. Both G3 and G4 use the RCP4.5 scenario for the baseline experiment and inject SO₂ every year from 2020 to 2070. The amount of SO₂ injected in G3 gradually increases to maintain the net radiative flux at the top-of-atmosphere (TOA) at the 2020 levels, while the radiative forcing of the greenhouse gases increases according to the RCP4.5 scenario. Conversely, in G4 the SO₂ injection rate is fixed at 5 Tg yr⁻¹. A summary of the G1–G4 studies is presented by Kravitz et al. (2013d) and the latest list of GeoMIP studies is available at <http://climate.envsci.rutgers.edu/GeoMIP/index.html>.

As summarized by Kravitz et al. (2013d), studies analysing GeoMIP experiments have explored and clarified climate model responses to radiative forcing and its dependence on various factors. In addition, the dependence (or uncertainty) of the direct forcing to the net surface SW induced by sulphate aerosol injection (hereafter SRM forcing) on models should be also studied



well, since estimation of the SRM forcing is important when considering the costs and benefits of geoengineering. The G1 and G2 experimental designs have limited utility in understanding sulphate aerosol geoengineering because the SRM is introduced simply and directly by the reduction of the solar constant. In G3, the amount of injected SO_2 mimicked in each model varies by year, which is useful for controlling the absolute amount of forcing but not the injection rate. In contrast, in G4 the rate of SO_2 injection is fixed at 5 Tg yr^{-1} throughout the SRM period, and the annually averaged strength of the SRM forcing should be almost constant during the SRM period in each model, but may differ among models. Therefore, the G4 experiment is suitable for directly exploring the strength and the model dependence or uncertainty of the SRM forcing.

There are numerous sources of inter-model differences in response to the same (or similar) forcing. On a broad scale, different models have distinct climate sensitivities and thus different global mean temperature responses to the same forcing. In addition, different models have various representations of processes, which affects the direct response to the forcing as well as different feedback from the responses. For example, cloud adjustments (Schmidt et al., 2012), sea ice changes (Moore et al., 2014), and stratospheric ozone changes (Pitari et al., 2014) are all known to affect the climate response to geoengineering through feedback. The ocean response operates on longer timescales and has also been shown to be important in understanding the response to geoengineering (Kravitz et al., 2013b). Yu et al. (2015) calculated the difference in globally and temporally averaged near-surface air temperature of G4 (over 2030–2069) from “baseline climate” (RCP4.5 over 2010–2029) and showed a standard deviation of up to $\pm 0.31 \text{ K}$ among models, while the model mean of the temperature difference was 0.28 K . Whilst the models in G4 assume the same rate of SO_2 injection, model responses to the SRM differ widely. Investigation into what causes such a large inter-model variability is very important for SRM simulation studies.

A simple procedure is used for quantifying the contributions of different types of SW feedback to the climate model response to geoengineering with stratospheric sulphate aerosols. We provide results for both global and local effects, focusing on cross-model commonalities and differences. Note that the cooling of the air temperature is determined by the energy balance among SW, longwave radiation (LW), sensible heat flux, and latent heat flux. However, the latter three are mainly determined by the air and/or surface temperature (Kleidon et al., 2015), and it is difficult to separate any feedback effects and responses from them. Hence, changes to the three amounts are considered as “responses” to the SRM’s cooling effect, and the forcing and feedback of SW are analysed. The following section describes the data and methods used in this study. Section 3 presents the results of the analyses followed by a short discussion. Summary and concluding remarks are provided in Section 4.

2 Data and methods

The models analysed in this study are listed in Table 1. Note that the method of simulating sulphate aerosols differs among the participating models. HadGEM2-ES and MIROC-ESM-CHEM-AMP calculate the formation of sulphate aerosols from SO_2 injected from the lower stratosphere on the equator. BNU-ESM, MIROC-ESM, and MIROC-ESM-CHEM use a prescribed aerosol optical depth (AOD), which is formulated as one fourth of the strength of the 1991 eruption of Mount Pinatubo following Sato et al. (1993) and provided in <http://climate.envsci.rutgers.edu/GeoMIP/geomipaod.html>. The annual cycle and latitudinal distribution of the prescribed AOD, which is zonally uniform, is shown in Fig. 1; this annual cycle is repeated every



year during the SRM period. In CanESM2, a constant field of AOD (~ 0.047) has been given to express the effect of the SO_2 injection. The MIROC-ESM, MIROC-ESM-CHEM, and MIROC-ESM-CHEM-AMP are based on the same framework but differ in their treatment of atmospheric chemistry. An online atmospheric chemistry module is coupled in the MIROC-ESM-CHEM and MIROC-ESM-CHEM-AMP, whereas MIROC-ESM is not coupled with the chemistry module. In the MIROC-ESM-CHEM, the prescribed AOD is used for the stratospheric sulphate aerosols and for the calculation of the surface area density of the sulphur. Conversely, the MIROC-ESM-CHEM-AMP fully calculates the chemistry and micro-physics of the stratospheric sulphate aerosol formation from SO_2 (a detailed description is presented in Sekiya et al., 2016).

Note that the following four models also participated in the GeoMIP-G4 experiment but are not used in this study. CSIRO Mk3L (Phipps et al., 2011, 2012) mimics the effect of SO_2 injection by reduction of the solar constant, so the method of analysis described below cannot be used. GEOSCCM (Rienecker et al., 2008) and ULAQ (Pitari et al., 2002) do not include an ocean model and the sea surface temperature is prescribed, so that the surface temperature decrease by the SRM is not simulated in a way that is conducive to the analyses undertaken. GISS-E2-R (Schmidt et al., 2006) has issues in its output of clear-sky SW flux at the surface that preclude the incorporation of this data in the analyses.

The model output variables used in this study are monthly means of surface air temperature, upwelling and downwelling SW fluxes at the surface and TOA for all-sky and clear-sky. The data for both experiments (RCP4.5 and G4) from the models listed in Table 1 with all ensemble members are used.

Since the SRM forcing is mainly induced by the reflection of the SW by stratospheric sulphate aerosols, the atmospheric reflection rate is very important. In order to consider the feedback on the SW due to the SRM forcing, the atmospheric absorption rate and the surface albedo are also important. To estimate these rates and the albedo from SW fluxes described in the previous paragraph, a single-layer atmospheric model of SW transfer used in Donohoe and Battisti (2011) (hereafter DB11) is applied. DB11's single-layer model assumes that a fraction R of the downwelling solar radiation flux at the TOA S is reflected back to space, and a fraction A is absorbed by the atmosphere at the same single layer. A fraction α of the transmitted radiation flux $S(1 - R - A)$ is then reflected by the surface. This reflected upwelling radiative flux is reflected back to the surface at the rate of R and absorbed at the rate of A at the atmospheric layer, and the remainder $S\alpha(1 - R - A)^2$ is transmitted to space. This process continues, forming an infinite geometric series, as shown in Fig. 1 of DB11; therefore, the TOA upwelling SW flux ($F_{\text{TOA}}^{\uparrow}$), surface downwelling SW flux ($F_{\text{SURF}}^{\downarrow}$), and surface upwelling SW flux ($F_{\text{SURF}}^{\uparrow}$) can be written as follows:

$$\begin{aligned}
 F_{\text{TOA}}^{\uparrow} &= S [R + \alpha(1 - R - A)^2 + \alpha^2 R(1 - R - A)^2 + \alpha^3 R^2(1 - R - A)^2 + \dots] \\
 &= SR + \alpha S(1 - R - A)^2 [1 + (\alpha R) + (\alpha R)^2 + \dots] = SR + \alpha S \frac{(1 - R - A)^2}{1 - \alpha R}, \quad (1)
 \end{aligned}$$

$$\begin{aligned}
 F_{\text{SURF}}^{\downarrow} &= S [(1 - R - A) + \alpha R(1 - R - A) + \alpha^2 R^2(1 - R - A) + \alpha^3 R^3(1 - R - A) + \dots] \\
 &= S(1 - R - A) [1 + (\alpha R) + (\alpha R)^2 + (\alpha R)^3 + \dots] = S \frac{(1 - R - A)}{1 - \alpha R}, \quad (2)
 \end{aligned}$$

$$F_{\text{SURF}}^{\uparrow} = \alpha F_{\text{SURF}}^{\downarrow} = \alpha S \frac{(1 - R - A)}{1 - \alpha R}. \quad (3)$$

Here, the infinite series in the second lines of Eqs. (1) and (2) converge to the final expression on the right-hand side because $\alpha R < 1$. The fractions R , A , and α are positive and less than unity. Note that, to the best of our knowledge, the idea of forming



the infinite geometric series from SW transfer between a single layer and the surface can be traced back to Rasool and Schneider (1971), who calculated the effect of aerosol on the global temperature by considering a single aerosol layer.

From Eqs. (1)–(3), R , A , and α can be calculated when S , $F_{\text{TOA}}^{\uparrow}$, $F_{\text{SURF}}^{\downarrow}$, and $F_{\text{SURF}}^{\uparrow}$ are given. Surface albedo α can be obtained immediately by Eq. (3) as

$$\alpha = \frac{F_{\text{SURF}}^{\uparrow}}{F_{\text{SURF}}^{\downarrow}}. \quad (4)$$

5 Substitution of the product of Eqs. (2) and (3) into Eq. (1) yields

$$R = \frac{SF_{\text{TOA}}^{\uparrow} - F_{\text{SURF}}^{\downarrow}F_{\text{SURF}}^{\uparrow}}{S^2 - F_{\text{SURF}}^{\downarrow 2}}, \quad (5)$$

for calculating the value of R . Then, A is calculated using values of R and α by the following form of Eq. (2):

$$A = (1 - R) - \frac{F_{\text{SURF}}^{\downarrow}}{S}(1 - \alpha R). \quad (6)$$

Note that, R , A , and α cannot be obtained when $S = 0$ such as during the polar night.

Based on the DB11's single-layer model described above, the strength of the SRM forcing and the effects of changes in the water vapour amount, cloud amount, and surface albedo are estimated using the method described in the remainder of this section. Since GeoMIP participating models provide all-sky and clear-sky values for $F_{\text{TOA}}^{\uparrow}$, $F_{\text{SURF}}^{\downarrow}$, and $F_{\text{SURF}}^{\uparrow}$, R , A , and α can be calculated for both all-sky and clear-sky; superscript "as" is used for all-sky and "cs" for clear-sky. Defining the cloud effects on a variable X by $X^{\text{cl}} \equiv X^{\text{as}} - X^{\text{cs}}$, the all-sky value is the sum of the clear-sky value and the cloud effect: $X^{\text{as}} = X^{\text{cs}} + X^{\text{cl}}$, where superscript "cl" is for the cloud effect. For further simplicity, the cloud effect on the surface albedo is assumed to be negligible (i.e., $\alpha^{\text{as}} \approx \alpha^{\text{cs}}$), and α^{as} is used in the following analyses and the superscript omitted. Now, the monthly mean of R^{cs} , R^{cl} , A^{cs} , A^{cl} , and α is calculated on each grid-point for RCP4.5 and G4 experiments.

Net SW at the surface is a key variable in this study and can be written as follows:

$$F_{\text{SURF}}^{\text{net}} \equiv F_{\text{SURF}}^{\downarrow \text{as}} - F_{\text{SURF}}^{\uparrow \text{as}} = (1 - \alpha)S \left[\frac{1 - (R^{\text{cs}} + R^{\text{cl}}) - (A^{\text{cs}} + A^{\text{cl}})}{1 - \alpha(R^{\text{cs}} + R^{\text{cl}})} \right]. \quad (7)$$

Here, $F_{\text{SURF}}^{\text{net}}$ is regarded as a function of S , R^{cs} , R^{cl} , A^{cs} , A^{cl} , and α . The difference of $F_{\text{SURF}}^{\text{net}}$ between RCP4.5 and G4 experiments is defined as

$$\Delta F_{\text{SURF}}^{\text{net}} \equiv F_{\text{SURF}}^{\text{net}}(S, R_{\text{G4}}^{\text{cs}}, R_{\text{G4}}^{\text{cl}}, A_{\text{G4}}^{\text{cs}}, A_{\text{G4}}^{\text{cl}}, \alpha_{\text{G4}}) - F_{\text{SURF}}^{\text{net}}(S, R_{\text{RCP}}^{\text{cs}}, R_{\text{RCP}}^{\text{cl}}, A_{\text{RCP}}^{\text{cs}}, A_{\text{RCP}}^{\text{cl}}, \alpha_{\text{RCP}}), \quad (8)$$

where the experiment names are indicated by subscripts "RCP" and "G4". (S , the TOA downwelling solar radiation, is same for RCP4.5 and G4.) Hereafter, $F_{\text{SURF}}^{\text{net}}(\text{RCP}) \equiv F_{\text{SURF}}^{\text{net}}(S, R_{\text{RCP}}^{\text{cs}}, R_{\text{RCP}}^{\text{cl}}, A_{\text{RCP}}^{\text{cs}}, A_{\text{RCP}}^{\text{cl}}, \alpha_{\text{RCP}})$ is written for convenience.

To estimate the strength of the SRM forcing and the effects of changes in the water vapour amount, cloud amount, and surface albedo on the net SW at the surface, the following is assumed:

1. The sulphate aerosols increased by the SO_2 injection amplify the reflection rate of the clear-sky atmosphere (R^{cs}), whilst their effect on the absorption rate (A^{cs}) is negligible.



2. The change in water vapour amount affects the absorption rate of the clear-sky atmosphere (A^{cs}), whilst its effect on the reflection rate (R^{cs}) is negligible.
 3. The amounts of other substances that affects the reflection or absorption rate of the clear-sky atmosphere do not change considerably, and their effects are negligible.
- 5 Though the sulphate aerosols can absorb near infrared radiation, which is a part of SW, its effect on the SRM forcing is ignored since its amount is insignificant compared to the SW reflected by the sulphate aerosols (Haywood and Ramaswamy, 1998). (An error due to ignoring the SW absorption by the sulphate aerosols is estimated at the end of this paper.)

Under the above assumptions, the strength of the SRM forcing F_{SRM} is defined by

$$F_{\text{SRM}} \equiv F_{\text{SURF}}^{\text{net}}(S, R_{\text{G4}}^{\text{cs}}, R_{\text{RCP}}^{\text{cl}}, A_{\text{RCP}}^{\text{cs}}, A_{\text{RCP}}^{\text{cl}}, \alpha_{\text{RCP}}) - F_{\text{SURF}}^{\text{net}}(\text{RCP}). \quad (9)$$

This is a change of net surface SW when only R^{cs} is changed to the value of G4. Similarly, the feedback effects from changes in the water vapour amount (E_{WV}), cloud amount (E_{C}), and surface albedo (E_{SA}) are defined as follows:

$$E_{\text{WV}} \equiv F_{\text{SURF}}^{\text{net}}(S, R_{\text{RCP}}^{\text{cs}}, R_{\text{RCP}}^{\text{cl}}, A_{\text{G4}}^{\text{cs}}, A_{\text{RCP}}^{\text{cl}}, \alpha_{\text{RCP}}) - F_{\text{SURF}}^{\text{net}}(\text{RCP}), \quad (10)$$

$$E_{\text{C}} \equiv F_{\text{SURF}}^{\text{net}}(S, R_{\text{RCP}}^{\text{cs}}, R_{\text{G4}}^{\text{cl}}, A_{\text{RCP}}^{\text{cs}}, A_{\text{G4}}^{\text{cl}}, \alpha_{\text{RCP}}) - F_{\text{SURF}}^{\text{net}}(\text{RCP}), \quad (11)$$

$$E_{\text{SA}} \equiv F_{\text{SURF}}^{\text{net}}(S, R_{\text{RCP}}^{\text{cs}}, R_{\text{RCP}}^{\text{cl}}, A_{\text{RCP}}^{\text{cs}}, A_{\text{RCP}}^{\text{cl}}, \alpha_{\text{G4}}) - F_{\text{SURF}}^{\text{net}}(\text{RCP}). \quad (12)$$

Here, the following three points should be noted. First, E_{WV} , E_{C} , and E_{SA} are measures for SW radiative feedback and do not include any LW effects; changes in the water vapour and cloud amounts can, however, affect LW transfer. Second, the sum of F_{SRM} , E_{WV} , E_{C} , and E_{SA} is not exactly equal to $\Delta F_{\text{SURF}}^{\text{net}}$, since Eq. (7) is not linear. However, if $\Delta F_{\text{SURF}}^{\text{net}} \approx F_{\text{SRM}} + E_{\text{WV}} + E_{\text{C}} + E_{\text{SA}}$ is satisfied, it can be stated that the decomposition of $\Delta F_{\text{SURF}}^{\text{net}}$ into F_{SRM} , E_{WV} , E_{C} , and E_{SA} is reasonable. Finally, E_{C} includes both the effect of changes in cloud cover and cloud albedo. This is because R^{cl} and A^{cl} can be written as follows, by expressing R^{as} and A^{as} with the total cloud-area fraction γ , the reflection rate of a fully cloud-covered atmosphere r^{fca} , and the absorption rate of a fully cloud-covered atmosphere a^{fca} ,

$$R^{\text{cl}} = R^{\text{as}} - R^{\text{cs}} = (1 - \gamma)R^{\text{cs}} + \gamma r^{\text{fca}} - R^{\text{cs}} = \gamma(r^{\text{fca}} - R^{\text{cs}}), \quad (13)$$

$$A^{\text{cl}} = A^{\text{as}} - A^{\text{cs}} = (1 - \gamma)A^{\text{cs}} + \gamma a^{\text{fca}} - A^{\text{cs}} = \gamma(a^{\text{fca}} - A^{\text{cs}}). \quad (14)$$

These expressions mean that cloud effects (R^{cl} and A^{cl}) include both the total cloud-area fraction and reflection or absorption rate of a fully cloud-covered atmosphere, which depends on cloud albedo or absorption rate. Therefore, E_{C} includes both the effect of changes in coverage, albedo and SW absorption rate of clouds. In addition, E_{C} should not include the “masking effect” (Zhang et al., 1994; Colman, 2003; Soden et al., 2004) of the clouds because the clear-sky values R^{cs} and A^{cs} are unchanged from those in RCP4.5.

In this study, the SRM forcing and the three feedback effects on net SW at the surface from the changes in the water vapour amount, cloud amount, and surface albedo, defined by Eqs. (9)–(12), are calculated on each grid-point where $S > 0$ from the monthly mean data. At grid points where $S = 0$, $F_{\text{SRM}} = E_{\text{WV}} = E_{\text{C}} = E_{\text{SA}} = 0$.



3 Results

3.1 Surface air temperature and shortwave radiation

Figure 2 shows the time series of globally averaged surface air temperature (hereafter, T) with a 12-month running mean for G4 (solid) and RCP4.5 (dashed). For all models, T in G4 decreases or remains at the 2020 level for a few decades and begins
5 increasing from around 2040 or earlier, whereas T in RCP4.5 steadily increases. Accordingly, the difference in T between RCP4.5 and G4 increases for a few decades from 2020 and then stops rising. That is, the cooling effect of SRM gradually affects the global mean of T because of slow feedback and/or thermal inertia of the modelled climate system, and takes a few decades to reach steady state. After that, the SRM becomes unable to prevent the temperature from increasing any more, delaying global warming for a few decades as compared with RCP4.5. In addition, after halting SRM at 2070, T increases
10 rapidly and then returns to the RCP4.5 level in each model. This rapid increase has been called the termination effect of SRM (e.g., Wigley, 2006; Jones et al., 2013; Kravitz et al., 2013d).

To properly compare the SRM effects among the models, we eliminate some of the transient behaviour and focus on the years 2040 to 2069, in which the amount of cooling in G4 compared with RCP4.5 is roughly kept constant. (Although the reason for the transient behaviour of the SRM's cooling effect is an important topic, it is beyond the scope of this study.) Figure
15 3 shows the relationship between ΔT ($\equiv T_{G4} - T_{RCP}$) and ΔF_{SURF}^{net} , the difference in net SW at the surface, averaged over the globe, for 2040–2069. For CanESM2, HadGEM2-ES, and MIROC-ESM-CHEM, the filled symbols indicate the ensemble mean whilst the unfilled symbols indicate individual ensemble members; for the other models, the filled symbols indicate the results of a single run. This figure shows a strong correlation between the mean ΔT and ΔF_{SURF}^{net} ; the correlation coefficient for the filled symbols is 0.88. This strong correlation allows ΔF_{SURF}^{net} to be used as a measure of the SRM effects, although
20 the surface air temperature depends on the energy balance among SW, LW, and sensible and latent heat fluxes at the surface. Therefore, in this study, SW is focused on for the estimation of the SRM forcing and the feedback from changes in the water vapour amount, cloud amount, and surface albedo, as described in the previous section.

3.2 Time-evolution of global mean forcing and SW feedbacks

The strength of the SRM forcing (F_{SRM}) defined by Eq. (9) and the SW feedback effects of changes in the water vapour amount
25 (E_{WV}), cloud amount (E_C), and surface albedo (E_{SA}) defined by Eqs. (10)–(12) are calculated for each model. Figure 4 shows the time-evolution of the globally averaged values of these measures with a 12-month running mean. ΔF_{SURF}^{net} and ΔT are also shown in this figure. In this subsection, the focus is on the qualitative features common to all or some of the models, whilst the quantitative differences are described in the following subsection.

In the models that used the prescribed or constant AOD field for the SRM (BNU-ESM, CanESM2, MIROC-ESM, and
30 MIROC-ESM-CHEM), F_{SRM} (red) immediately reaches a model-dependent negative value after 2020 and remains almost constant; it then vanishes instantly after the termination. These features are consistent with the fact that the given AOD for the SRM was instantly added and removed in these models. Conversely, in the models that calculate the formation and transport of the sulphate aerosols from the injected SO_2 (HadGEM2-ES and MIROC-ESM-CHEM-AMP), F_{SRM} takes approximately



four years to become saturated. During the period in which SRM is imposed, F_{SRM} in MIROC-ESM-CHEM-AMP is almost constant, but F_{SRM} in HadGEM2-ES varies by approximately 1.0 W m^{-2} .

The values of E_{SA} shown by the green curves are both negative and small in all of the models. This shows that, at least for the global average, the surface albedo under G4 is higher than that under RCP4.5. However, changes in the surface albedo do not significantly affect $\Delta F_{\text{SURF}}^{\text{net}}$.

Both E_{WV} and E_{C} are positive, implying that the changes in the water vapour amount and cloud amount reduce the cooling effect of the SRM. Temperature reduction decreases the amount of evaporation compared with the RCP4.5 scenario and results in less water vapour in the atmosphere (Kravitz et al., 2013c). Less water vapour can cause reduced cloud amounts; less water vapour and reduced cloud amounts increase the atmospheric SW transmissivity and reduce the SRM's cooling effect. The strengths of E_{WV} and E_{C} are comparable in each model except MIROC-ESM-CHEM-AMP. After SRM termination, E_{WV} remains positive for one or two decades. This is consistent with changes in ΔT shown by the dashed curves; i.e., the water vapour amount in G4 remains less than that in RCP4.5 for a while after the termination. The inter-annual variability of E_{C} is much larger than that of E_{WV} , and the gradual transition to the state of RCP4.5 after the termination (like E_{WV}) is not apparent. Through the whole simulation period, the inter-annual variability of E_{C} dominates that of $\Delta F_{\text{SURF}}^{\text{net}}$. It should be noted that the phases in wave-like, year-to-year variability of $\Delta F_{\text{SURF}}^{\text{net}}$ and ΔT (shown by black solid line and dashed line in Fig. 4) do not agree, although time-averaged $\Delta F_{\text{SURF}}^{\text{net}}$ is well correlated with ΔT as shown in Fig. 3. This is because of thermal inertia and nonlinearities in the Earth system.

3.3 Inter-model dispersion of global mean forcing and SW feedbacks

For the inter-model comparison of the results, the global means of F_{SRM} , E_{WV} , E_{C} , and E_{SA} were averaged over the period 2040–2069. Figure 5 shows the relationship between these values (y-axis) and ΔT (x-axis) in the same manner as Fig. 3; $\Delta F_{\text{SURF}}^{\text{net}}$ is shown again. The mean values of F_{SRM} (shown by red symbols) vary widely from approximately -3.6 to -1.6 W m^{-2} , depending on the model. The cooling effect of F_{SRM} in each member or the ensemble mean is reduced by the heating effects of E_{WV} (orange) and E_{C} (blue) and is slightly increased by E_{SA} (green). The net effect is approximately equal to $\Delta F_{\text{SURF}}^{\text{net}}$ (black), which is strongly correlated with ΔT ; the residual is less than 0.06 W m^{-2} . This supports the validity of the decomposition of $\Delta F_{\text{SURF}}^{\text{net}}$ into SRM forcing and the effects of changes in the water vapour amount, cloud amount, and surface albedo.

The two models with sulphate aerosol calculation (HadGEM2-ES and MIROC-ESM-CHEM-AMP) show stronger F_{SRM} than the others. This outcome indicates that the prescribed AOD, which is based on one-fourth of the Mount Pinatubo eruption, likely underestimates the AOD that results from actual SO_2 injection at a rate of 5 Tg yr^{-1} .

In CanESM2 and MIROC-ESM-CHEM, the F_{SRM} values are comparable among the ensemble members shown by unfilled red symbols. This is consistent with the fact that the given AOD fields for mimicking the SO_2 injection effects in G4 are identical among ensemble members of each model. On the other hand, the values of F_{SRM} in the ensemble members of HadGEM2-ES have considerable differences, because the distribution of the sulphate AOD is affected by the chaotic nature of transport and various other processes in the ESM.



Pitari et al. (2014) have shown that SW radiative forcing at the tropopause calculated off-line by a radiative transfer code (Chou and Suarez, 1999; Chou et al., 2001) varies from around -2.1 to -1.0 W m^{-2} . Since both the analysis methods and the participating models presented here differ from those of Pitari et al., it is difficult to compare the two results. However, the results ($F_{\text{SRM}} \sim -3.6$ to -1.6 W m^{-2}) show that model dependence of the SRM forcing might be larger than that shown by Pitari et al.

Figure 5 shows that E_{WV} is strongly anti-correlated with ΔT ; the correlation coefficient for the filled symbols is -0.94 . In contrast, E_{C} seems to have no correlation with ΔT , with a correlation coefficient of 0.01 . This result shows that the SW feedback effect from the change in water vapour amount is much simpler (i.e., almost linear with ΔT across all models) than that from changing the cloud amount, which depends strongly on the cloud parameterization scheme. Furthermore, the results of the ensemble members of CanESM2 and MIROC-ESM-CHEM show that the variation in E_{C} mainly causes the variation in $\Delta F_{\text{SURF}}^{\text{net}}$, which is well correlated with ΔT , though F_{SRM} is same among the members. Thus, among the ensemble members, higher E_{C} seems to bring less cooling. MIROC-ESM-CHEM-AMP marks the strongest forcing of the SRM among the models but also marks the largest heating effect from changing the cloud amount. Accordingly, this model shows the moderate values in $\Delta F_{\text{SURF}}^{\text{net}}$ and ΔT ; a possible explanation is given in the following analysis.

To compare ratios of the feedback and the surface cooling to the magnitude of the SRM forcing, E_{WV} , E_{C} , E_{SA} , and ΔT by $|F_{\text{SRM}}|$ were normalized, as shown in Fig. 6. This figure shows the approximate sensitivity of each feedback per unit forcing of SRM (y-axis) and the normalized surface cooling (x-axis). The value range of $E_{\text{C}}/|F_{\text{SRM}}|$ (0.19 – 0.55 , blue) is significantly wider than that of $E_{\text{WV}}/|F_{\text{SRM}}|$ (0.27 – 0.42 , orange) and that of $E_{\text{SA}}/|F_{\text{SRM}}|$ (-0.12 to -0.06 , green). In addition, the three MIROC-based models show higher $E_{\text{C}}/|F_{\text{SRM}}|$ (0.34 – 0.55) than other three models (0.19 – 0.34). This means that the sensitivity of the feedback effect due to change in cloud amount in the MIROC-based models is higher than other models. This may be why MIROC-ESM-CHEM-AMP, whose $E_{\text{C}}/|F_{\text{SRM}}|$ is as high as those of MIROC-ESM and MIROC-ESM-CHEM, exhibits high E_{C} and yields moderate cooling, although F_{SRM} is very strong, as shown by the cross sign in Fig. 5. That is, high sensitivity of E_{C} to the SRM forcing will weaken the cooling of surface air temperature as well as $\Delta F_{\text{SURF}}^{\text{net}}$.

The wide variability of $E_{\text{C}}/|F_{\text{SRM}}|$ among the models implies a large uncertainty in the models' cloud processes. Moreover, the spread of $E_{\text{C}}/|F_{\text{SRM}}|$ among nine ensemble members of MIROC-ESM-CHEM is also large. The variability among the ensemble members implies that the cloud amount is considerably affected by the chaotic properties and high sensitivity to the initial state of the Earth system or ESM. This result therefore suggests that the cooling of the surface air temperature by the SRM depends significantly on the initial state through feedback due to changes in the cloud amount.

3.4 Robust features in geographical distribution

To explore robust features in the effects of the SRM in G4, the multi-model mean of the surface air temperature and net SW at the surface is calculated. Figures 7a and 7b show ΔT and $\Delta F_{\text{SURF}}^{\text{net}}$ averaged over the period 2040–2069; hatching indicates regions where 4 (out of 6) or fewer models agreed on the sign of the difference. The zonal means are shown in the right-hand side panel for each variable (black indicates the multi-model mean, and coloured lines indicate the ensemble mean of each model). The geographical distribution of the multi-model mean shows that cooling of the surface air temperature is very strong



in and around the Arctic Region, except for Greenland and Europe, and stronger on land than over the ocean in other regions. Reduction of $F_{\text{SURF}}^{\text{net}}$ is strong in the eastern part of Southern Africa, Tibet, East Asia, Sea of Okhotsk, Hudson Bay, and South America. In contrast, $F_{\text{SURF}}^{\text{net}}$ increased compared with RCP4.5 in the equatorial region of the Western Pacific, Southern Ocean, except near the Antarctic coast and northern part of the Atlantic. The above reduction and increase are mainly due to E_C and E_{SA} ; details will be discussed later in this section. The spatial distribution of the sign of $\Delta F_{\text{SURF}}^{\text{net}}$ varies, whereas ΔT is negative over the whole globe. Although ΔT and $\Delta F_{\text{SURF}}^{\text{net}}$ are correlated in the global mean (Fig. 3), the spatial distribution of ΔT does not necessarily need to agree with that of $\Delta F_{\text{SURF}}^{\text{net}}$ because circulation and hydrological processes transport and redistribute energy.

Qualitatively opposite geographical features in ΔT and $\Delta F_{\text{SURF}}^{\text{net}}$ appear in the simulated climate change in RCP4.5 shown in Figs. 7c and 7d, calculated as the difference between the 2010–2039 average and the 2040–2069 average of the RCP4.5 data. Note that the very high positive value in East Asia in Fig. 7d is due to a large reduction of anthropogenic aerosol emission assumed in the late 21st century in the RCP4.5 scenario (Thomson et al., 2011; Westervelt et al., 2015). With the exception of the effects of such assumed emission reduction, sulphate geoengineering can delay global warming almost without regional biases; that is, regions where surface air temperature increases are relatively high in RCP4.5 undergo a large amount of cooling by the sulphate geoengineering and regions with a relatively low increases in temperature receive a small amount of cooling. Model dependence in ΔT shown by coloured lines in Fig. 7a is relatively large in high latitudes in the Northern Hemisphere but small (i.e., comparable with the spread of the global mean ΔT) in other regions. For $\Delta F_{\text{SURF}}^{\text{net}}$ shown in Fig. 7b, all models show qualitatively similar average features at least in the zonal mean, and the range is about $\pm 0.75 \text{ W m}^{-2}$.

Next, the multi-model mean of global distributions (averaged over 2040–2069) of (a) F_{SRM} , (b) E_{WV} , (c) E_C , and (d) E_{SA} are calculated, as shown in Fig. 8. The SRM forcing is relatively weak in the regions where the annual mean surface albedo is high, such as Greenland, the Sahara, the Middle East, Australia, and Antarctica. This is mainly because the net SW at the surface is low due to the high surface albedo, and accordingly the absolute value of the SRM forcing becomes low. This can be shown via low order approximation: the net SW at the surface can be written as $F_{\text{SURF}}^{\text{net}} \approx (1 - \alpha)S(1 - R - A)$, and the SRM forcing can be approximated as $F_{\text{SRM}} \approx -(1 - \alpha_{\text{RCP}})S(R_{\text{G4}}^{\text{cs}} - R_{\text{RCP}}^{\text{cs}})$, whose absolute value becomes small when α_{RCP} is high. Except for these high surface-albedo regions, the spatial variation in SRM forcing is not very large, even though the incoming solar radiation is strong at low latitudes and weak at high latitudes. This is because the atmospheric reflection rate depends on the solar zenith angle, and the reflection rate becomes higher as the zenith angle increases (e.g., Joseph et al., 1976). That is, strong solar radiation at low latitudes is reflected with low efficiency and weak solar radiation at the high latitudes is reflected with high efficiency. Accordingly, the latitudinal distribution of the SRM forcing is close to uniform (except for MIROC-ESM-CHEM-AMP, whose distribution of sulphate aerosols is not as uniform as the prescribed AOD); see the red line graph in Fig. 8a. The above feature is a notable aspect in sulphate geoengineering compared with idealized SRM experiments such as G1 and G2, which simply reduced the solar constant (Kravitz et al., 2013a).

The SW feedback of the change in the water vapour amount (Fig. 8b) is close to uniform compared with that of the cloud amount (Fig. 8c). E_C has a large spatial variability, which yields many of the spatial variation of $\Delta F_{\text{SURF}}^{\text{net}}$, such as positive values in the equatorial region of the Western Pacific, the Southern Ocean, and the northern part of the Atlantic, and negative



values in the eastern part of the Southern Africa, East Asia, and South America. Because $\Delta F_{\text{SURF}}^{\text{net}}$ (Fig. 7b) and the simulated climate change of $F_{\text{SURF}}^{\text{net}}$ in RCP4.5 (Fig. 7d) are opposite in sign, the above result suggests that the SRM offsets increases in the cloud amount simulated in the RCP4.5 scenario, in the positive regions in Fig. 8c and vice versa in the negative regions. The remaining features in $\Delta F_{\text{SURF}}^{\text{net}}$ are caused by the effect of surface albedo change (Fig. 8d), which has large negative values in Tibet, the Sea of Okhotsk, Hudson Bay, and the Southern Ocean near the Antarctic coast. That is, snow and sea ice remain in these regions in the G4 experiment because of the SRM. At high latitudes, the cooling effect of the change in surface albedo is as strong as the heating effect of the change in cloud amount (see the line graph in panels c and d), although E_{SA} is minor in the global mean.

4 Summary and concluding remarks

The results from six models (listed in Table 1) that simulated GeoMIP experiment G4, which is designed to simulate sulphate geoengineering by injecting 5 Tg of SO_2 into the stratosphere every year from 2020 to 2070 in the RCP4.5 scenario as the baseline, have been analysed. A single-layer model proposed by Donohoe and Battisti (2011) has been applied to estimate the strength of the SRM forcing (F_{SRM}) to the surface net shortwave radiation, whose difference between G4 and RCP4.5 ($\Delta F_{\text{SURF}}^{\text{net}}$) has a strong correlation with the cooling of the surface air temperature (ΔT), as shown in Fig. 3. The SW feedback effects of changes in the water vapour amount (E_{WV}), cloud amount (E_{C}), and surface albedo (E_{SA}) have been also estimated.

It has been shown that the globally and temporally averaged F_{SRM} of each model varies widely from about -3.6 to -1.6 W m^{-2} (red symbols in Fig. 5). Inter-model variations comprise a substantial range, and narrowing this uncertainty is essential for understanding the effects of sulphate geoengineering and its interactions with chemical, micro-physical, dynamical, and radiative processes related to the formulation, distribution, and shortwave-reflectance of the sulphate aerosols introduced from the SO_2 injection.

Our analysis has also shown that the SW feedback from changes in the water vapour and cloud amounts (from RCP4.5) reduce the cooling effect of F_{SRM} by approximately $0.4\text{--}1.2 \text{ W m}^{-2}$ and $0.5\text{--}1.5 \text{ W m}^{-2}$, respectively. This is due to the smaller amounts of water vapour and clouds, which mainly block the downwelling solar radiation from reaching the surface by absorption and reflection, respectively. E_{WV} is well correlated with ΔT in multi-model comparison, whereas E_{C} is not. The reduction rate of E_{C} varies from 19 % to 55 % as compared to F_{SRM} depending on both models and ensemble runs (i.e., initial states), whereas that of E_{WV} is 27–42 %. Therefore, uncertainty of the feedback due to changes in the cloud amount would be dominant for the cooling effect under the same F_{SRM} . This means that improvements in the representation of cloud processes is also needed for an accurate simulation of SRM. The effect of surface albedo changes is small in the global average, but is significant in the regions where snow or ice melts in the RCP4.5 scenario.

The multi-model mean horizontal distribution of ΔT suggests that stratospheric sulphate aerosol geoengineering can delay global warming without significant regional biases, unlike the results of the GeoMIP-G1 experiment (Kravitz et al., 2013a). In G1, the incoming solar radiation was just reduced by a constant fraction, so that the SRM forcing has large latitudinal variation (strong in low-latitudes and weak in high-latitudes). Conversely, in G4, the distribution of sulphate aerosol optical depth (AOD)



is internally calculated or externally given, and the reflection of the solar radiation is locally calculated. Here, at least for the prescribed AOD calculated from observed AOD after the 1991 Mount Pinatubo eruption, sulphate aerosols are assumed to spread out globally and form a somewhat uniform distribution as shown in Fig. 1. Because the reflection rate, as well as the incoming solar radiation, depends on the solar zenith angle, as described previously, the resultant SRM forcing does not have large latitudinal variation, as shown in Fig. 8a.

This study has the following four limitations. First, the single-layer model used treats the reflection of downward radiation and that of upward radiation by the same rate. As noted above, however, the reflection rate depends on the incident angle, so errors could be significant in regions that have high solar zenith angle and high surface albedo, such as Greenland and Antarctica.

Second, half of the models used in this study have only one ensemble member, and half are MIROC-based models. Because the numbers of ensemble members differ among models as listed in Table. 1, each member in each model is not equally weighted in calculation of the multi-model means described in Section 3.4. Responses to the SRM forcing in three MIROC-based models should be similar to each other as shown in Fig. 6, so that the results of multi-model mean can be biased to that of the MIROC-based models.

Third, the SW absorption by the sulphate aerosols has been ignored, because its amount is considered minor compared to the SW reflection. If the absorption by the sulphate aerosols is non-negligible, E_{WV} should be regarded as the sum of a part of SRM forcing by absorption and feedback from the change in the water vapour amount, and the forcing and feedback are not well separated from each other. At least for MIROC-ESM-CHEM, this study confirms that the influence of SW absorption by the sulphate aerosols on E_{WV} is less than 4.5 % by performing the G4 experiment with vanishing SW absorption coefficients of the sulphate aerosols. In other words, the SRM forcing due to SW absorption by the sulphate aerosols is less than 1.5 % of that due to reflection (F_{SRM}). The magnitude of errors in the other models should be similar to that in MIROC-ESM-CHEM.

Finally, only SW has been analysed and the energy balance has not been considered. ΔT can be affected by other types of feedback, e.g., the less water vapour and reduced cloud amounts in G4 can reduce the greenhouse effect in the LW transfer and contribute to temperature cooling. Analyses of the full energy balance and other types of feedback will form part of future work.

5 Data availability

All data used in this study, except for the data of MIROC-ESM-CHEM-AMP, are available through the Earth System Grid Federation (ESGF) Network (<http://esgf.llnl.gov>). The data of MIROC-ESM-CHEM-AMP are available by contacting the corresponding author.

Author contributions. HK, MA, SW, and TS analysed the data. SW, TS, DJ, JM, and JC developed the models and performed the experiment. BK designed and organized the experiment. All authors contributed to the discussion.

The authors declare that they have no conflict of interest.



Acknowledgements. We thank all participants of the Geoengineering Model Intercomparison Project and their model development teams, CLIVAR/WCRP Working Group on Coupled Modelling for endorsing GeoMIP, and the scientists managing the Earth System Grid data nodes who have assisted with making GeoMIP output available. We thank Drs. Charles Curry, James M. Haywood, and Andy Jones for model development and comments on the manuscript. We also thank Drs. Masahiro Sugiyama, Hideo Shiogama, and Seita Emori for useful comments. HK, MA, and SW were supported by the SOUSEI Program, MEXT, Japan. Simulations of MIROC-based models were conducted using the Earth Simulator. The Pacific Northwest National Laboratory is operated for the U.S. Department of Energy by Battelle Memorial Institute under contract DE-AC05-76RL01830.



References

- Arora, V. K. and Boer, G. J.: Uncertainties in the 20th century carbon budget associated with land use change, *Glob. Change Biol.*, 16, 3327–3348, 2010.
- Arora, V. K., Scinocca, J. F., Boer, G. J., Christian, J. R., Denman, K. L., Flato, G. M., Kharin, V. V., Lee, W. G., and Merryfield, W. J.: Carbon emission limits required to satisfy future representative concentration pathways of greenhouse gases, *Geophys. Res. Lett.*, 38, L05805, 2011.
- Bala, G., Duffy, P. B., and Taylor, K. E.: Impact of geoengineering schemes on the global hydrological cycle., *P. Natl. Acad. Sci. USA*, 105, 7664–7669, 2008.
- Budyko, M. I.: *Climate and life*, Academic Press, New York, 1974.
- Chou, M. D. and Suarez, M. J.: A solar radiation parameterization for atmospheric studies, Tech. Rep. TM-1999-104606, NASA Goddard Space Flight Center, Greenbelt, MD, 1999.
- Chou, M.-D., Suarez, M. J., Liang, X.-Z., Yan, M. M. H., and Cote, C.: A thermal infrared radiation parameterization for atmospheric studies, Tech. Rep. TM-2001-104606, NASA Goddard Space Flight Center, Greenbelt, MD, 2001.
- Collins, W. J., Bellouin, N., Doutriaux-Boucher, M., Gedney, N., Halloran, P., Hinton, T., Hughes, J., Jones, C. D., Joshi, M., Liddicoat, S., Martin, G., O'Connor, F., Rae, J., Senior, C., Sitch, S., Totterdell, I., Wiltshire, A., and Woodward, S.: Development and evaluation of an Earth-System model – HadGEM2, *Geosci. Model Dev.*, 4, 1051–1075, 2011.
- Colman, R.: A comparison of climate feedbacks in general circulation models, *Clim. Dynam.*, 20, 865–873, 2003.
- Crutzen, P. J.: Albedo enhancement by stratospheric sulfur injections: A contribution to resolve a policy dilemma?, *Climatic Change*, 77, 211–220, 2006.
- Donohoe, A. and Battisti, D. S.: Atmospheric and surface contributions to planetary albedo, *J. Climate*, 24, 4402–4418, 2011.
- Govindasamy, B. and Caldeira, K.: Geoengineering Earth's radiation balance to mitigate CO₂-induced climate change, *Geophys. Res. Lett.*, 27, 2141–2144, 2000.
- Govindasamy, B., Thompson, S., Duffy, P. B., Caldeira, K., and Delire, C.: Impact of geoengineering schemes on the terrestrial biosphere, *Geophys. Res. Lett.*, 29, 2002.
- Govindasamy, B., Caldeira, K., and Duffy, P. B.: Geoengineering Earth's radiation balance to mitigate climate change from a quadrupling of CO₂, *Global Planet. Change*, 37, 157–168, 2003.
- Haywood, J. M. and Ramaswamy, V.: Global sensitivity studies of the direct radiative forcing due to anthropogenic sulfate and black carbon aerosols, *J. Geophys. Res.*, 103, 6043–6058, 1998.
- IPCC: *Climate Change 2007: Synthesis Report, Contribution of working groups I, II and III to the Fourth Assessment Report of the Intergovernmental Panel on Climate Change*, IPCC, Geneva, 2007.
- Ji, D., Wang, L., Feng, J., Wu, Q., Cheng, H., Zhang, Q., Yang, J., Dong, W., Dai, Y., Gong, D., Zhang, R. H., Wang, X., Liu, J., Moore, J. C., Chen, D., and Zhou, M.: Description and basic evaluation of Beijing Normal University Earth System Model (BNU-ESM) version 1, *Geosci. Model Dev.*, 7, 2039–2064, 2014.
- Jones, A., Haywood, J., Boucher, O., Kravitz, B., and Robock, A.: Geoengineering by stratospheric SO₂ injection: results from the Met Office HadGEM2 climate model and comparison with the Goddard Institute for Space Studies ModelE, *Atmos. Chem. Phys.*, 10, 5999–6006, 2010.



- Jones, A., Haywood, J. M., Alterskjær, K., Boucher, O., Cole, J. N. S., Curry, C. L., Irvine, P. J., Ji, D., Kravitz, B., Egill Kristjánsson, J., Moore, J. C., Niemeier, U., Robock, A., Schmidt, H., Singh, B., Tilmes, S., Watanabe, S., and Yoon, J. H.: The impact of abrupt suspension of solar radiation management (termination effect) in experiment G2 of the Geoengineering Model Intercomparison Project (GeoMIP), *J. Geophys. Res.-Atmos.*, 118, 9743–9752, 2013.
- 5 Joseph, J. H., Wiscombe, W. J., and Weinman, J. A.: The delta-Eddington approximation for radiative flux transfer, *J. Atmos. Sci.*, 33, 2452–2459, 1976.
- Kleidon, A., Kravitz, B., and Renner, M.: The hydrological sensitivity to global warming and solar geoengineering derived from thermodynamic constraints, *Geophys. Res. Lett.*, 42, 138–144, 2015.
- Kravitz, B., Robock, A., Boucher, O., Schmidt, H., Taylor, K. E., Stenchikov, G., and Schulz, M.: The Geoengineering Model Intercomparison Project (GeoMIP), *Atmos. Sci. Lett.*, 12, 162–167, 2011.
- 10 Kravitz, B., Caldeira, K., Boucher, O., Robock, A., Rasch, P. J., Alterskjær, K., Karam, D. B., Cole, J. N. S., Curry, C. L., Haywood, J. M., Irvine, P. J., Ji, D., Jones, A., Kristjánsson, J. E., Lunt, D. J., Moore, J. C., Niemeier, U., Schmidt, H., Schulz, M., Singh, B., Tilmes, S., Watanabe, S., Yang, S., and Yoon, J. H.: Climate model response from the Geoengineering Model Intercomparison Project (GeoMIP), *J. Geophys. Res.-Atmos.*, 118, 8320–8332, 2013a.
- 15 Kravitz, B., Forster, P. M., Jones, A., Robock, A., Alterskjær, K., Boucher, O., Jenkins, A. K. L., Korhonen, H., Kristjánsson, J. E., Muri, H., Niemeier, U., Partanen, A.-I., Rasch, P. J., Wang, H., and Watanabe, S.: Sea spray geoengineering experiments in the geoengineering model intercomparison project (GeoMIP): Experimental design and preliminary results, *J. Geophys. Res.-Atmos.*, 118, 11,175–11,186, 2013b.
- Kravitz, B., Rasch, P. J., Forster, P. M., Andrews, T., Cole, J. N. S., Irvine, P. J., Ji, D., Kristjánsson, J. E., Moore, J. C., Muri, H., Niemeier, U., Robock, A., Singh, B., Tilmes, S., Watanabe, S., and Yoon, J. H.: An energetic perspective on hydrological cycle changes in the Geoengineering Model Intercomparison Project, *J. Geophys. Res.-Atmos.*, 118, 13,087–13,102, 2013c.
- 20 Kravitz, B., Robock, A., Forster, P. M., Haywood, J. M., Lawrence, M. G., and Schmidt, H.: An overview of the Geoengineering Model Intercomparison Project (GeoMIP), *J. Geophys. Res.-Atmos.*, 118, 13,103–13,107, 2013d.
- Lane, L., Caldeira, K., Chatfield, R., and Langhoff, S., eds.: Workshop report on managing solar radiation, 2007.
- 25 Matthews, H. D. and Caldeira, K.: Transient climate–carbon simulations of planetary geoengineering, *P. Natl. Acad. Sci. USA*, 104, 9949–9954, 2007.
- Moore, J. C., Rinke, A., Yu, X., Ji, D., Cui, X., Li, Y., Alterskjær, K., Kristjánsson, J. E., Muri, H., Boucher, O., Huneus, N., Kravitz, B., Robock, A., Niemeier, U., Schulz, M., Tilmes, S., Watanabe, S., and Yang, S.: Arctic sea ice and atmospheric circulation under the GeoMIP G1 scenario, *J. Geophys. Res.-Atmos.*, 119, 567–583, 2014.
- 30 Parker, D. E., Wilson, H., Jones, P. D., Christy, J. R., and Folland, C. K.: The impact of mount Pinatubo on world-wide temperatures, *Int. J. Climatol.*, 16, 487–497, 1996.
- Phipps, S. J., Rotstayn, L. D., Gordon, H. B., Roberts, J. L., Hirst, A. C., and Budd, W. F.: The CSIRO Mk3L climate system model version 1.0 – Part 1: Description and evaluation, *Geosci. Model Dev.*, 4, 483–509, 2011.
- Phipps, S. J., Rotstayn, L. D., Gordon, H. B., Roberts, J. L., Hirst, A. C., and Budd, W. F.: The CSIRO Mk3L climate system model version 1.0 – Part 2: Response to external forcings, *Geosci. Model Dev.*, 5, 649–682, 2012.
- 35 Pitari, G., Mancini, E., Rizi, V., and Shindell, D. T.: Impact of future climate and emission changes on stratospheric aerosols and ozone, *J. Atmos. Sci.*, 59, 414–440, 2002.



- Pitari, G., Aquila, V., Kravitz, B., Robock, A., Watanabe, S., Cionni, I., Luca, N. D., Genova, G. D., Mancini, E., and Tilmes, S.: Stratospheric ozone response to sulfate geoengineering: Results from the Geoengineering Model Intercomparison Project (GeoMIP), *J. Geophys. Res.-Atmos.*, 119, 2629–2653, 2014.
- Rasch, P. J., Crutzen, P. J., and Coleman, D. B.: Exploring the geoengineering of climate using stratospheric sulfate aerosols: The role of particle size, *Geophys. Res. Lett.*, 35, L02809, 2008.
- Rasool, S. I. and Schneider, S. H.: Atmospheric carbon dioxide and aerosols: Effects of large increases on global climate, *Science*, 173, 138–141, 1971.
- Rienecker, M. M., Suarez, M. J., Todling, R., Bacmeister, J., Takacs, L., Liu, H. C., Gu, W., Sienkiewicz, M., Koster, R. D., Gelaro, R., Stajner, I., and Nielsen, J. E.: The GEOS-5 data assimilation system-documentation of versions 5.0.1, 5.1.0, and 5.2.0, Technical Report Series on Global Modeling and Data Assimilation, 27, 2008.
- Robock, A., Oman, L., and Stenchikov, G. L.: Regional climate responses to geoengineering with tropical and Arctic SO₂ injections, *J. Geophys. Res.*, 113, D16101, 2008.
- Sato, M., Hansen, J. E., and McCormick, M. P.: Stratospheric aerosol optical depths, 1850–1990, *J. Geophys. Res.*, 98, 22 987–22 994, 1993.
- Schmidt, G. A., Ruedy, R., Hansen, J. E., Aleinov, I., Bell, N., Bauer, M., Bauer, S., Cairns, B., Canuto, V., Cheng, Y., Del Genio, A., Faluvegi, G., Friend, A. D., Hall, T. M., Hu, Y., Kelley, M., Kiang, N. Y., Koch, D., Lacis, A. A., Lerner, J., Lo, K. K., Miller, R. L., Nazarenko, L., Oinas, V., Perlwitz, J., Perlwitz, J., Rind, D., Romanou, A., Russell, G. L., Sato, M., Shindell, D. T., Stone, P. H., Sun, S., Tausnev, N., Thresher, D., and Yao, M.-S.: Present-day atmospheric simulations using GISS ModelE: Comparison to in situ, satellite, and reanalysis data, *J. Climate*, 19, 153–192, 2006.
- Schmidt, H., Alterskjær, K., Bou Karam, D., Boucher, O., Jones, A., Kristjánsson, J. E., Niemeier, U., Schulz, M., Aaheim, A., Benduhn, F., Lawrence, M., and Timmreck, C.: Solar irradiance reduction to counteract radiative forcing from a quadrupling of CO₂: climate responses simulated by four earth system models, *Earth Syst. Dynam.*, 3, 63–78, 2012.
- Sekiya, T., Sudo, K., and Nagai, T.: Evolution of stratospheric sulfate aerosol from the 1991 Pinatubo eruption: Roles of aerosol microphysical processes, *J. Geophys. Res.-Atmos.*, 2016.
- Shepherd, J. G.: *Geoengineering the climate: science, governance and uncertainty*, Royal Society, 2009.
- Soden, B. J., Broccoli, A. J., and Hemler, R. S.: On the use of cloud forcing to estimate cloud feedback, *J. Climate*, 17, 3661–3665, 2004.
- Thomson, A. M., Calvin, K. V., Smith, S. J., Kyle, G. P., Volke, A., Patel, P., Delgado-Arias, S., Bond-Lamberty, B., Wise, M. A., Clarke, L. E., and Edmonds, J. A.: RCP4.5: a pathway for stabilization of radiative forcing by 2100, *Climatic Change*, 109, 77–94, 2011.
- Watanabe, S., Hajima, T., Sudo, K., Nagashima, T., Takemura, T., Okajima, H., Nozawa, T., Kawase, H., Abe, M., Yokohata, T., Ise, T., Sato, H., Kato, E., Takata, K., Emori, S., and Kawamiya, M.: MIROC-ESM 2010: model description and basic results of CMIP5-20c3m experiments, *Geosci. Model Dev.*, 4, 845–872, 2011.
- Westervelt, D. M., Horowitz, L. W., Naik, V., Golaz, J. C., and Mauzerall, D. L.: Radiative forcing and climate response to projected 21st century aerosol decreases, *Atmos. Chem. Phys.*, 15, 12 681–12 703, 2015.
- Wigley, T. M. L.: A combined mitigation/geoengineering approach to climate stabilization, *Science*, 314, 452–454, 2006.
- Yu, X., Moore, J. C., Cui, X., Rinke, A., Ji, D., Kravitz, B., and Yoon, J. H.: Impacts, effectiveness and regional inequalities of the GeoMIP G1 to G4 solar radiation management scenarios, *Global Planet. Change*, 129, 10–22, 2015.
- Zhang, M. H., Hack, J. J., Kiehl, J. T., and Cess, R. D.: Diagnostic study of climate feedback processes in atmospheric general circulation models, *J. Geophys. Res.*, 99, 5525–5537, 1994.

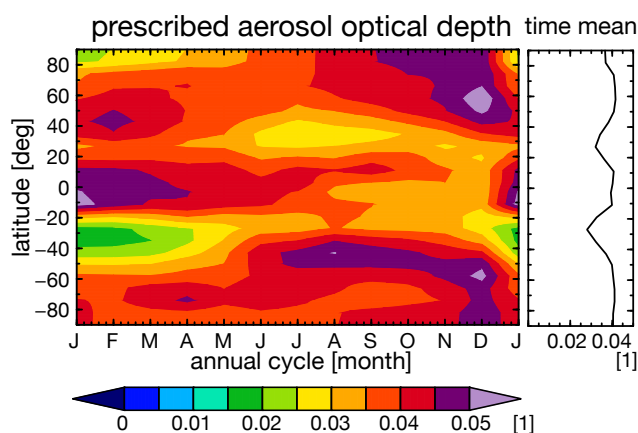


Figure 1. Annual cycle and latitudinal distribution of the prescribed aerosol optical depth provided from the GeoMIP for G4 experiment and used in BNU-ESM, MIROC-ESM, and MIROC-ESM-CHEM. Line graph shows the annual mean.

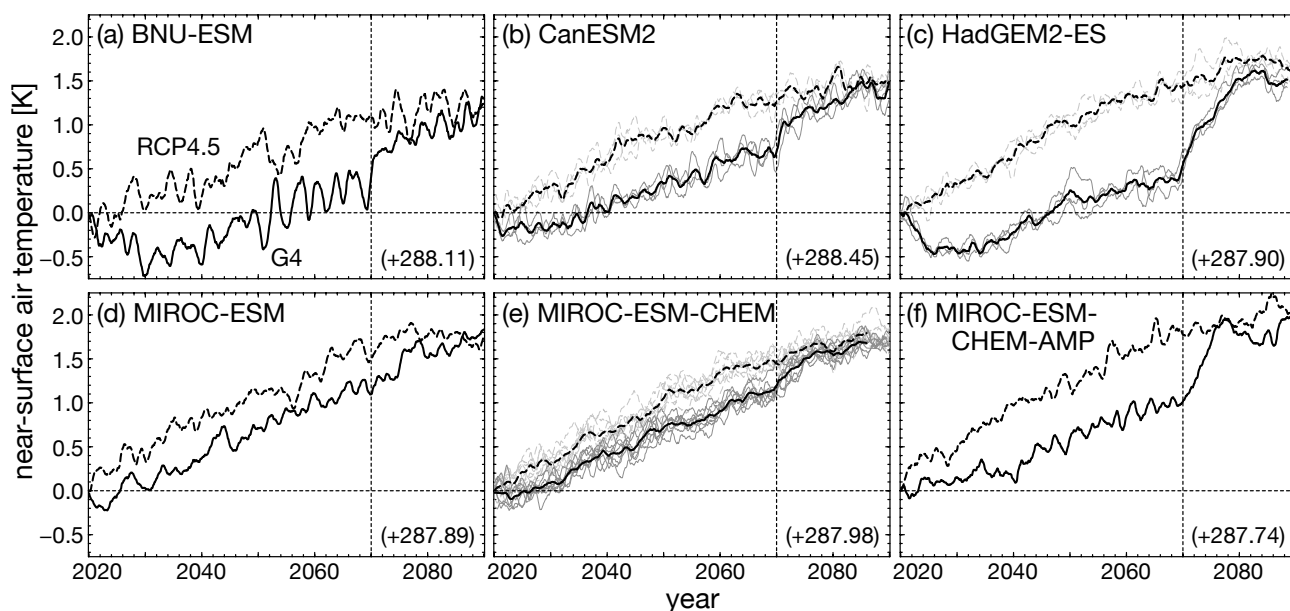


Figure 2. Globally averaged surface air temperature in G4 (solid) and RCP4.5 (dashed) experiments. 12-month running mean is applied. Values are offset by the value at 2020, the beginning of SRM, shown at the right bottom on each panel. In panels (b), (c), and (e), black curves show the ensemble mean and grey curves show ensemble members. The vertical dashed lines indicate the SRM termination (2070).

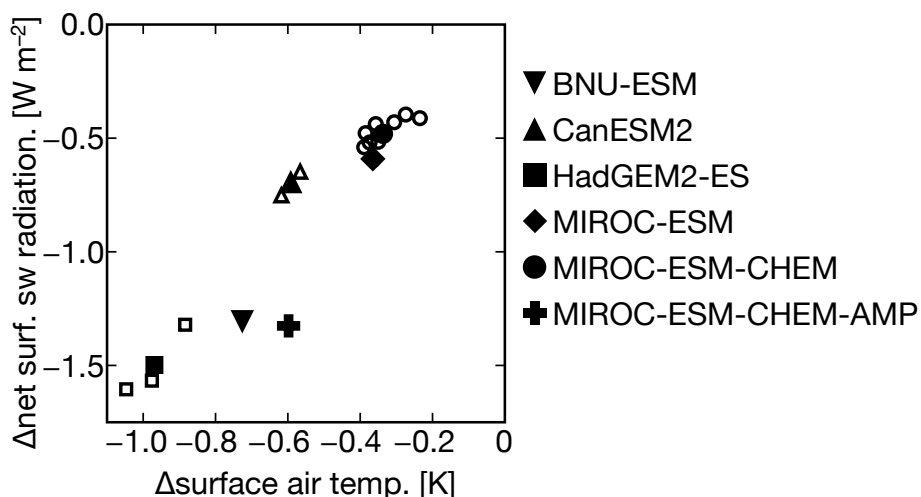


Figure 3. Relationship between the difference in the globally and temporally averaged surface air temperature (x-axis) and that of the net shortwave radiation at the surface (y-axis). The term of average is from 2040 to 2069. For CanESM2, HadGEM2-ES, and MIROC-ESM-CHEM, the ensemble mean is shown by filled symbols and the each member by unfilled ones.

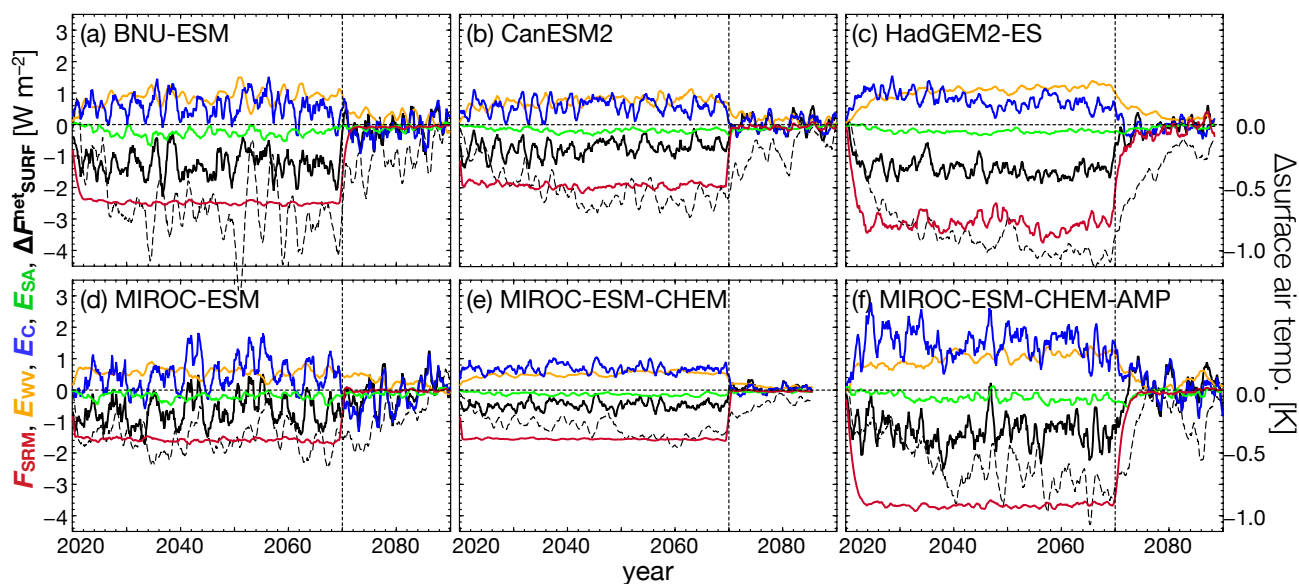


Figure 4. Same as Fig. 2 but for the SRM forcing (red), SW feedback due to changes in the water vapour (orange), cloud amounts (blue), and surface albedo (green) defined in Eqs. (9–12), and the difference in the net shortwave radiation at the surface (black, solid). The difference in the surface air temperature is also plotted by dashed-black curves whose values are shown by the right axis.

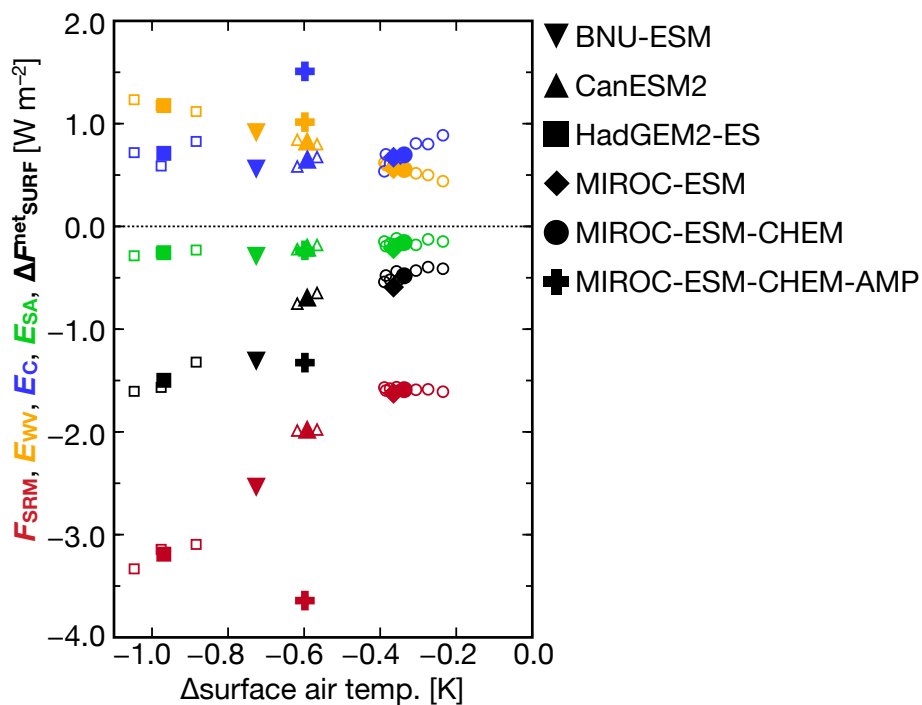


Figure 5. Same as Fig. 3 but also for SRM forcing (red), SW feedback due to changes in the water vapour amount (orange), cloud amount (blue), and surface albedo (green).

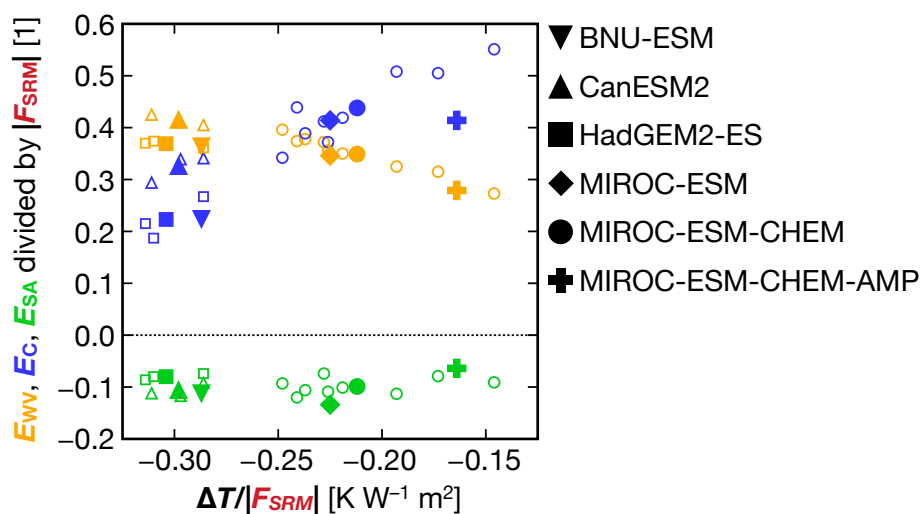


Figure 6. Same as Fig. 5 but for the SW feedback effects normalized by the absolute value of the SRM forcing. Note that the difference in the surface air temperature (x-axis) is also divided by $|F_{SRM}|$.

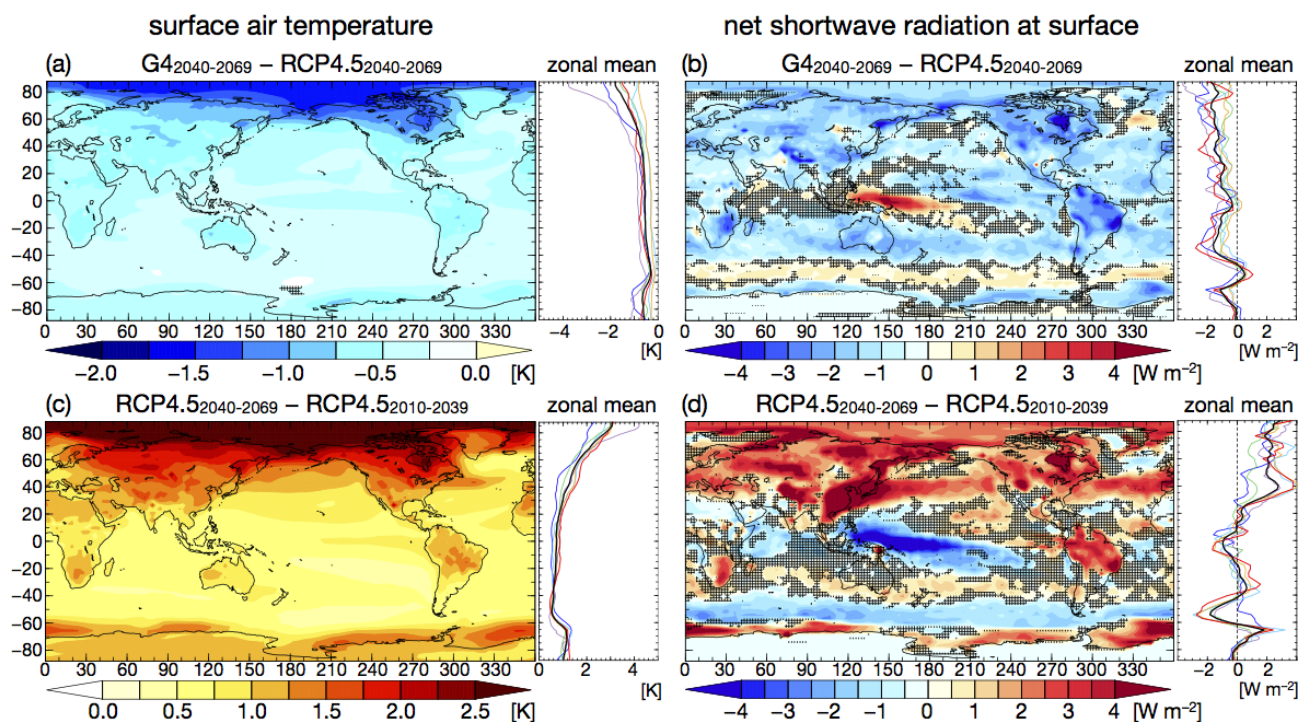


Figure 7. Multi-model mean of difference in the surface air temperature and net shortwave radiation at the surface. Panels (a) and (b) show the difference between G4 and RCP4.5 averaged over 2040–2069. Panels (c) and (d) show the difference between RCP4.5 averaged over 2040–2069 and that over 2010–2039. The colour tone shows the horizontal distribution and the black line on the right-hand side shows the zonal mean of the multi-model mean. Other coloured lines display the ensemble mean (or the result of the single run) of each model (blue: BNU-ESM, green: CanESM2, purple: HadGEM2-ES, cyan: MIROC-ESM, orange: MIROC-ESM-CHEM, red: MIROC-ESM-CHEM-AMP). Hatching indicates the region where 4 (out of 6) or fewer models agreed on the sign of the difference.

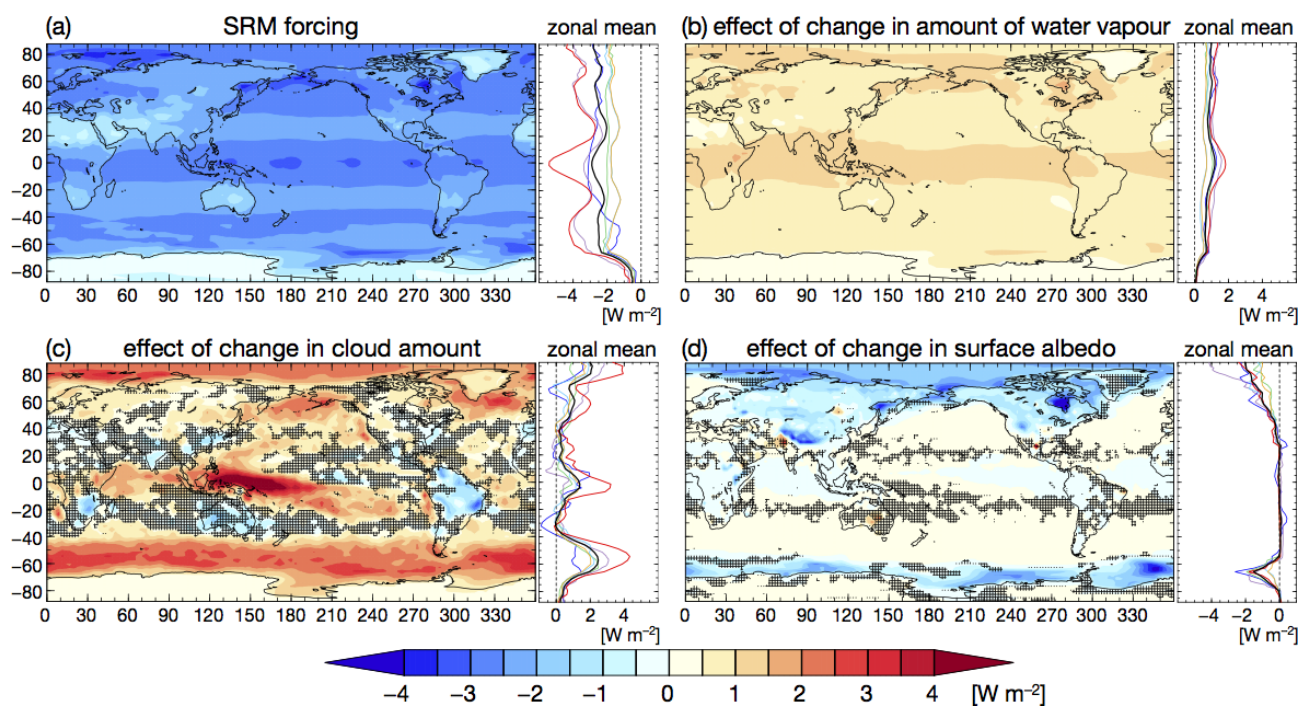


Figure 8. Same as Fig. 7 but for multi-model mean of (a) SRM forcing, SW feedback due to changes in the (b) water vapour amount, (c) cloud amount, and (d) surface albedo, averaged over 2040–2069.



Table 1. Models participating in GeoMIP G4 experiments and used in this study. Manners of simulating sulphate aerosol optical depth (AOD) and ensemble members are shown for each model.

Models	Sulfate AOD	Ensemble Members
BNU-ESM Ji et al. (2014)	Prescribed	1
CanESM2 Arora and Boer (2010); Arora et al. (2011)	Uniform	3
HadGEM2-ES Collins et al. (2011)	Internally Calculated	3
MIROC-ESM Watanabe et al. (2011)	Prescribed	1
MIROC-ESM-CHEM Watanabe et al. (2011)	Prescribed	9
MIROC-ESM-CHEM-AMP Watanabe et al. (2011); Sekiya et al. (2016)	Internally Calculated	1